Manuscript Details

Manuscript number	ENVPOL_2017_2524
Title	Size-segregated aerosol in a hot-spot pollution urban area: Chemical composition and three-way source apportionment
Article type	Research Paper

Abstract

In this work, a comprehensive characterisation and source apportionment of size-segregated aerosol collected using a multistage cascade impactor was performed. The samples were collected during wintertime in Milan (Italy), which is located in the Po Valley, one of the main pollution hot-spot areas in Europe. For every sampling, size-segregated mass concentration, elemental and ionic composition, and levoglucosan concentration were determined. Size-segregated data were inverted using the program MICRON to identify and quantify modal contributions of all the measured components. The detailed chemical characterisation allowed the application of a three-way (3-D) receptor model (implemented using Multilinear Engine) for size-segregated source apportionment and chemical profiles identification. It is noteworthy that - as far as we know - this is the first time that three-way source apportionment is attempted using data of aerosol collected using traditional cascade impactors. Seven factors were identified: wood burning, industry, resuspended dust, regional aerosol, construction works, traffic 1, and traffic 2. Further insights into size-segregated factor profiles suggested that the traffic 1 factor can be associated to diesel vehicles and traffic 2 to gasoline vehicles. The regional aerosol factor resulted to be the main contributor (nearly 50%) to the droplet mode (accumulation sub-mode with modal diameter in the range 0.5-1 μm), whereas the overall contribution from the two factors related to traffic was the most important one in the other size modes (34-41%). The results showed that applying a 3-D receptor model to size-segregated samples allows identifying factors of local and regional origin while receptor modelling on integrated PM fractions usually singles out factors characterised by primary (e.g. industry, traffic, soil dust) and secondary (e.g. ammonium sulphate and nitrate) origin. Furthermore, the results suggested that the information on size-segregated chemical composition in different size classes was exploited by the model to relate primary emissions to rapidly-formed secondary compounds.

Keywords	Multistage cascade impactor; aerosol size distribution; size-segregated chemical composition; three-way source apportionment; gasoline vehicles; diesel vehicles

Corresponding Author	Roberta Vecchi
Order of Authors	Vera Bernardoni, Miriam Elser, Gianluigi Valli, Sara Valentini, Alessandro Bigi, PAOLA FERMO, Andrea Piazzalunga, Roberta Vecchi

Suggested reviewers	Peter Molnár, Fulvio Amato, claudio Belis, Wioletta Rogula-Kozłowska, Imre SALMA

Size-segregated aerosol in a hot-spot pollution urban area: Chemical composition and three-way source apportionment

V. Bernardoni[1], M. Elser[1,#], G. Valli[1], S. Valentini[1], A. Bigi[2], P. Fermo[3], A. Piazzalunga[3,§], R. Vecchi[1,*]

[1]Dipartimento di Fisica, Università degli Studi di Milano and INFN-Milan, Milan, Italy

[2]Dipartimento di Ingegneria "Enzo Ferrari", Università degli Studi di Modena e Reggio Emilia, Modena, Italy

[3]Dipartimento di Chimica, Università degli Studi di Milano, Milan, Italy

[#]now at: Swiss Federal Laboratories for Materials Science and Technology, Empa, Dübendorf, Switzerland

[§]now at: Water & Life Lab, Entratico (BG), Italy

*Corresponding Author:
Prof. Roberta Vecchi
Dipartimento di Fisica
Università degli Studi di Milano
Via Celoria 16
20133 Milan
Italy
tel: +39 02 50317498
email: roberta.vecchi@unimi.it

Abstract

In this work, a comprehensive characterisation and source apportionment of size-segregated aerosol collected using a multistage cascade impactor was performed. The samples were collected during wintertime in Milan (Italy), which is located in the Po Valley, one of the main pollution hot-spot areas in Europe.

For every sampling, size-segregated mass concentration, elemental and ionic composition, and levoglucosan concentration were determined. Size-segregated data were inverted using the program MICRON to identify and quantify modal contributions of all the measured components.

The detailed chemical characterisation allowed the application of a three-way (3-D) receptor model (implemented using Multilinear Engine) for size-segregated source apportionment and chemical profiles identification. It is noteworthy that - as far as we know - this is the first time that three-way source apportionment is attempted using data of aerosol collected using traditional cascade impactors. Seven factors were identified: wood burning, industry, resuspended dust, regional

aerosol, construction works, traffic 1, and traffic 2. Further insights into size-segregated factor profiles suggested that the traffic 1 factor can be associated to diesel vehicles and traffic 2 to gasoline vehicles. The regional aerosol factor resulted to be the main contributor (nearly 50%) to the droplet mode (accumulation sub-mode with modal diameter in the range 0.5-1 μm), whereas the overall contribution from the two factors related to traffic was the most important one in the other size modes (34-41%).

The results showed that applying a 3-D receptor model to size-segregated samples allows identifying factors of local and regional origin while receptor modelling on integrated PM fractions usually singles out factors characterised by primary (e.g. industry, traffic, soil dust) and secondary (e.g. ammonium sulphate and nitrate) origin. Furthermore, the results suggested that the information on size-segregated chemical composition in different size classes was exploited by the model to relate primary emissions to rapidly-formed secondary compounds.

Capsule: detailed chemical characterisation of samples collected by multistage cascade impactor was performed. Application of three-way receptor model allowed obtaining size-segregated source apportionment.

Keywords: Multistage cascade impactor; aerosol size distribution; size-segregated chemical composition; three-way source apportionment; gasoline vehicles; diesel vehicles

1. Introduction

Atmospheric aerosol is a complex mixture of solid and liquid particles suspended in the atmosphere. Atmospheric aerosol has impacts at local scale on health (e.g. Pope and Dockery, 2006), visibility (e.g. Watson, 2002), cultural heritage damage (e.g. Bonazza et al., 2005) and at global scale on the Earth radiation balance (IPCC, 2013). The main parameters determining the aerosol effects are particle sizes and chemical properties, which depend on source emissions and following transformations/reactions in atmosphere (Pöschl, 2005). As examples, size-segregated information can be used to gain further insights into aerosol effects on health (Heal et al., 2012) and can be exploited in perspective to improve Earth radiative transfer models.

Atmospheric aerosol can be separated in several size-ranges and collected for subsequent analysis using multistage cascade impactors. Measurement techniques for the characterisation of different components of size-segregated aerosol have been described in the literature (e.g. Maenhaut et al., 1999 for elemental analysis by Particle-Induced X-ray emission; Viidanoja et al., 2002 for organic and elemental carbon analysis). To provide complete chemical characterisation, sampling on different filter media is mandatory (e.g. Maenhaut et al., 2002; Rogula-Kozłowska, 2016; Salma et

al., 2005). Nevertheless, sampling using cascade impactors is not straightforward, mainly due to the number of samples to deal with. Thus, it can be worthy developing non-destructive, traditional techniques (e.g. ED-XRF) to provide a relatively wide chemical characterisation on the same sample with no need of unconventional laboratory devices (e.g. accelerators).

Information on aerosol sources can be obtained from physical-chemical characterisation of aerosol collected in ambient air e.g. using multivariate receptor models (Hopke, 2016; Viana et al., 2008; and therein cited literature), which allow to retrieve aerosol source contributions, chemical profiles, and temporal trends. Three-way (3-D) source apportionment models (Harshman and Lundy, 1994; Tucker, 1966) can be applied to size- and time-resolved aerosol samples to obtain information on size-segregated source profiles and contributions. Nevertheless, in spite of the importance of exploiting information on size-segregated aerosol composition for source apportionment purposes, studies concerning a comprehensive characterisation of aerosol segregated in more than two size classes coupled to 3-D source apportionment are nearly absent in the literature. Few examples are applications to data collected using a high-resolution time-of-flight mass spectrometer - HR-ToF-MS (Ulbrich et al., 2012) or drum impactors (Li et al., 2013; Peré-Trepat et al., 2007). Nevertheless, the high cost and complex operation of the HR-ToF-AMS and the need of accelerator facilities for the elemental analysis of drum impactor samples (Bukowiecki et al., 2005; Cahill, 1996) strongly limit the spatial and temporal applicability of these techniques.

In this work, a comprehensive characterisation of size-segregated aerosol collected using a multistage cascade impactor was performed quantifying mass by gravimetry, elements by ED-XRF, main inorganic ions and levoglucosan by liquid chromatographic techniques. The detailed size-segregated characterisation allowed the determination of mass and chemical components size distribution at a heavily polluted area (Milan, Italy). Furthermore, a 3-D receptor model (implemented using Multilinear Engine) was applied to obtain size-segregated source profiles and apportionment from samples collected using traditional multistage cascade impactors. As far as we know, this is the first time that 3-D source apportionment is attempted on this kind of data.

2. Materials and Methods

2.1 Sampling

Aerosol was sampled using a multistage cascade impactor collecting particles in 12-stages with nominal cut-off diameter in the range 45 nm - 8.5 μm (SDI, Dekati - more details in Bernardoni et al., 2011a). Samples were collected on coated polycarbonate substrates to avoid particle bouncing among impaction stages. Coating was performed using DS-515 spray by Dekati. Upstream the impactor, a PM10 EPA-equivalent inlet was used. It is noteworthy to recall that EPA inlets are designed to perform a 10 μm cut-off at 16.67 l/min. Considering the SDI flow-rate (11.12 l/min),

106 the expected size-cut of the inlet in this work was calculated to be 12.2 μm.
107 Samplings were performed at an urban background site in the University Campus in the period
108 January-March 2011. Fourteen samplings were performed with a time resolution in the range 24-48
109 h, for a total of 168 polycarbonate foils available for the analysis.
110 During the sampling period, median temperature was 7.4°C (range: -2.7°C to 20.0°C, except for the
111 last three samplings when temperatures up to 24°C were reached). Average wind speed was 0.72
112 m/s. Wind speed higher than 4 m/s were occasionally registered during a Foehn event (15th
113 February). Precipitations occurred during 1 sampling only, with a rate lower than 2 mm/h. The
114 integral precipitation during that sampling was 6.4 mm.
115
116 ***2.2 Laboratory analyses***
117 All the substrates were weighed before and after the sampling using an analytical microbalance
118 (precision 1 μg) in an air-conditioned weighing room (T = 20 ± 1°C and R.H. = 50 ± 5%). Before
119 weighing, filters were placed on open but dust-protected sieve-trays for 48 hours in the weighing
120 room for conditioning. The weighing protocol is described in Vecchi et al. (2004). Calibration
121 procedures checked the microbalance performance.
122 Elemental composition (S, Cl, K, Ca, Ti, V, Cr, Mn, Fe, Ni, Cu, Zn, Br, Pb) was determined on all
123 samples using an Energy-Dispersive X-Ray Fluorescence instrument (ED-2000, Oxford) suitably
124 set up for the analysis of samples collected using multistage cascade impactors (details in
125 Bernardoni et al., 2011a). Minimum detection limits were in the range 1-20 ng/sample, depending
126 on the considered element (except for S and Cl: 140 and 89 ng/sample, respectively), corresponding
127 to about 0.1-8.9 ng/m^3 when considering sampling volumes. Uncertainties were estimated in the
128 range 7-15% for most elements and samples.
129 After ED-XRF analysis, which is fully not destructive, all the samples were water extracted for the
130 determination of the main inorganic ions ($SO_4^=$, NO_3^-, NH_4^+, K^+) and levoglucosan. Extraction of
131 each sample was performed using 30 μl methanol and 3 ml MilliQ water, sonicating for 1 h. The
132 main inorganic ions were determined by ion chromatography (details in Piazzalunga et al., 2013).
133 Minimum detection limits were 25 ng/sample for ammonium (0.7-1.6 ng/m^3 depending on sampling
134 volume), 100 ng/sample for sulphate and nitrate (3.2-7.3 ng/m^3), and 170 ng/sample for potassium
135 (5.4-12.3 ng/m^3). Uncertainties were about 10%. Levoglucosan measurements were performed by
136 high-performance liquid chromatography coupled to pulsed-amperometric detection (HPAEC–
137 PAD) (details in Piazzalunga et al., 2010). Minimum detection limit was 11 ng/sample (0.4-0.8
138 ng/m^3) and uncertainties were about 10%.
139
140 ***2.3 Modes retrieval by the program MICRON.***

For each measured component, size segregated concentration measured by multistage impactors is usually represented as histogram (see Figure 1a). Each bar of the histogram is related to the characteristics of the considered impactor stage and of the collected aerosol as follows: the bar width (represented in log-scale) extends from the cut-off of considered stage and the cut-off of the previous one (i.e. the adjacent stage with higher cut-off); the bar height represents $\Delta m/\Delta \log(d_p)$ where Δm is the component mass measured on the considered stage and $\Delta \log(d_p)$ is the difference between the logarithms of the cut-off diameters of the previous and considered stages. When a continuous distribution is of interest, $dm/d(\log(d_p))$ as a function of d_p are represented (note that when $\log(d_p)$ is used, it has to be intended as $\log(d_p/d_{p0})$, where d_{p0}=1μm, for details see Seinfeld and Pandis, 1998). Nevertheless, a more accurate representation of the original size distribution has to take into account real cut-off curves of the impactor. To this aim, the inversion program MICRON (Wolfenbarger and Seinfeld, 1990) was used to retrieve the original size distribution of the different chemical components for each sampling (see Figure 1b). The inversion is based on a constrained regularisation algorithm. Model inputs are the mass/species concentrations collected on each impaction stage, which are redistributed considering the actual collection efficiency of the SDI impactor (Hillamo, 1994) and the uncertainties on input data. Each inverted $dm/d(\log(d_p))$ distribution is then fitted with log-normal functions (see Figure 1c) to retrieve the geometric mean aerodynamic diameter (GMAD), and the different contributions of the modes (Maenhaut et al., 1996).

2.4 Source apportionment

Source apportionment was performed using a vector-matrix decomposition, inspired to the Tucker1 model (Tucker, 1966). In this model, each element $x_{i,j,k}$ of the 3-D input matrix representing the M species of the aerosol collected in N stages of a cascade impactor during R samplings is factorised in S (unknown) factors as follows: $x_{i,j,k}=\sum_{p=1}^{S} b_{i,j,p} a_{p,k} + \varepsilon_{i,j,k}$, where $\varepsilon_{i,j,k}$ is the difference between the measured and the modelled concentrations. Different meanings can be attributed to the factorising terms (Ulbrich et al., 2012). In our decomposition, $b_{i,j,p}$ ($1 \le i \le N$, $1 \le j \le M$, $1 \le p \le S$) was an element of an N×M×S array, where each N×M layer represents the size-segregated p-th factor profile and $a_{p,k}$ ($1 \le k \le R$) represents the contribution of the p-th factor to the k-th sampling.

The model was implemented using Multilinear Engine - ME-2 (Paatero, 1999) and is based on the minimisation of the object function $Q = \sum_i \sum_j \sum_k \frac{\varepsilon_{i,j,k}^2}{\sigma_{i,j,k}^2}$, where $\sigma_{i,j,k}$ is the uncertainty associated to each $x_{i,j,k}$. The function Q previously reported represents the main equation of the model. Further constraints can be applied by adding other terms (auxiliary equations). The conjugate gradient

algorithm is used to compute the solution. Non-negativity constraints are implemented by using the well-known technique of pre-conditioning in opposite way for slowing down changes of variables that are about to become negative. Factor scaling indeterminacy can be removed including a priori information on factor matrices. In our case, normalisation was carried out as follows: $\sum_k a_{p,k} = 1$ for each factor p.

The model was run using strong variables (Paatero 2015). This excluded Cr and Ni. S and $SO_4^=$ showed very good correlation and correct stoichiometric ratio. $SO_4^=$ was chosen because of the higher associated explained mass. The choice between K^+ and K was performed considering that they were very well correlated for d≤2.70 μm but K provided significant contribution also in larger size fractions (due to insoluble K related e.g. to potassium oxides in crustal material). Thus, K was chosen as input. Cl resulted with no other tracers in a single factor accounting for few mass thus preventing physical interpretation. Summarising, twelve variables were chosen as input data: K, Ca, Ti, Mn, Fe, Cu, Zn, levoglucosan, $SO_4^=$, NO_3^-, NH_4^+, and mass. It is noteworthy that carbonaceous material was not measured so that unexplained mass (i.e. the difference between the mass and the detected species) ranged from 34% to >95% depending on the sample. Generally, the highest unexplained mass was registered in very small size classes: this was consistent with the small size expected for carbonaceous particles emitted from combustion processes.

Data and uncertainties were treated following Polissar et al. (1998). In our case, $\sigma_{i,j,k}$ was the analytical uncertainty associated to the chemical species. Exception was the uncertainty associated to the mass as it was increased to 4-times the mass value. Indeed, mass was considered as "total variable", i.e. it was used to determine factor scaling and for source contribution quantification. Total variable should not have strong influence on the solution, thus it should be always down-weighed (EPA, 2014).

Species were measured in 168 samples. Data were arranged into a 3-D matrix representing 12 size classes × 12 species × 14 samplings. Missing data were identified as -999 and were automatically excluded by the program in the computation of the Q function. Due to the unknown number of factors, solutions for different numbers of factors were explored to identify the best solution. Multiple minima are a crucial issue in 3-D models. Thus, the global minimum and a few of the deepest local minima were explored (Paatero, 2000).

3. Results and discussion

3.1 Mass and chemical components size distribution

All the size-segregated data concerning mass and chemical components for all the samplings were inverted using the program MICRON as explained in paragraph 2.3.

For what concerns aerosol mass, two different types of mass size distributions were detected in the measured data (see Figure 2). They mainly differed in the absence (type 1) or presence (type 2) of a detectable Aitken mode at about 100 nm. The presence of the Aitken mode has probably to be ascribed to samples impacted by fresh and local emissions and its absence to a more aged aerosol. Some literature works argued the possibility of vapour condensation during low-pressure impactor sampling due to expansion cooling. Nevertheless, Raabe et al. (1988) did not found it as an issue considering that the lower temperature is reached instantaneously and maintained only for short time (of the order of μs). When present, the Aitken mode accounted on average for 9% of the measured mass.

For d > 100 nm, the mass size distribution showed the accumulation mode separated into two sub-modes (condensation mode and droplet mode, e.g. see Seinfeld and Pandis, 1998) and the coarse mode. GMADs for condensation, droplet, and coarse modes were 0.28 μm, 0.72 μm, 4.1 μm, respectively, for mass size distribution type 1; for mass size distribution type 2, GMADs for the three modes were 0.29 μm, 0.71 μm, 3.7 μm. Mode GMADs were very similar to previously literature findings (e.g. Cabada et al., 2004; Salma et al., 2005). Whether no significant differences in mode GMADs were present between the two size distribution types, the relative contribution of condensation and droplet modes was different: indeed, in mass size distribution type 1 the contribution of the droplet mode was significantly higher than in the other case. This observation and the absence of the Aitken mode evidenced the role of aging processes leading to the increase of particle sizes.

Modal distributions for all the measured chemical components were retrieved. Condensation, accumulation, and coarse modes, as well as very large particles were detected for most species, whereas Aitken nuclei mode was detected for levoglucosan, NO_3^-, $SO_4^=$, and K^+. Results concerning these modes GMADs, relative mass concentration (RMC) (when modes were present), and the relative number of cases in which modes occurred were summarised in Table 1. Furthermore, an "intermediate mode" (not shown in Table 1) with 0.9 μm ≤ GMAD ≤1.2 μm was detected in more than 85% cases for Ca, Ti, Fe, Cu, and in 36% cases for Ni. When present, the intermediate mode accounted for less than 25% of the total mass of the species. An intermediate mode was already found for Ca, Ti, and Fe at urban sites in the literature (Pakkanen et al., 2001; Salma et al., 2005), where coal combustion (not expected to impact the samples presented in this work), regional, and mineral aerosol related to road dust were mentioned as possible origin of the mode.

It is noteworthy that information on the size distribution of chemical components is very important e.g. to provide information useful for the assessment of aerosol health effects and to constrain inputs to Earth radiative transfer models.

In Figure 3a, the size distribution for secondary inorganic ions was shown. The droplet mode clearly prevailed on the condensation mode consistently with previous findings in the literature (e.g. Cabada et al., 2004), where gas-phase reactions were identified as responsible for the condensation mode formation. Heterogeneous formation, cloud processing, and growth of the condensation mode were indicated as processes leading to droplet mode increase. In addition, secondary inorganic ions presented the Aitken mode (4% relative contribution $SO_4^{=}$, 2% for NH_4^+ and NO_3^-). In the literature, direct emission of ultrafine inorganic ions (especially sulphate) were associated to combustion processes, as traffic (e.g. Robert et al., 2007) or wood/pellets burning (Ozgen et al., 2017).
In Figure 3b, levoglucosan, K^+, and elemental K concentrations were shown. They are known tracers for wood burning (Kleeman et al., 1999; Simoneit et al., 1999; Viana et al., 2008). As expected, K gave a higher contribution than K^+ because it referred to total (i.e. soluble plus insoluble) potassium concentration in atmospheric aerosol. Focusing on $d_p < 1$ μm, the major contribution for wood burning tracers was found in the accumulation sub-modes (as previously observed for secondary inorganic ions) but here the condensation mode dominated on the droplet mode, indicating different formation processes for particles containing these compounds compared to secondary inorganic ions. Furthermore, the presence of the Aitken mode suggested the likely impact of local (urban) emissions by wood/pellet burning. Indeed, recent literature works reported emissions of ultrafine particles containing levoglucosan by wood stoves and K^+ by wood and pellet stoves (Ozgen et al., 2017). Ultrafine particles containing K and levoglucosan were identified also in ambient aerosol in relationship to residential wood burning (Corsini et al., 2017; Pirjola et al., 2017). For $d_p > 1$μm, a much higher contribution from K than from K^+ can be noticed indicating the contribution from insoluble potassium to be likely ascribed to crustal elements.
Figure 3b and Figure 3c represented markers wood burning and traffic sources (among the main sources identified in the Milan urban area in previous works – e.g. Bernardoni et al., 2011b). It is noteworthy that the size distributions for tracers of the two sources are completely different. Opposite, smaller differences are registered among species considered as tracers for the same source. Thus, 3-D receptor modelling was applied trying to exploit these differences to gain further details on emission sources.

3.2 Receptor model results

The Tucker 1 model was implemented in ME-2 as explained in paragraph 2.4. Receptor models are always affected by multiple solutions for what concerns the possible number of factors, scaling indeterminacy, local minima, and possibly rotations (not an issue in 3-D models). Some mathematical parameters were checked to identify a range of possible solution (expected vs. computed Q value, residuals distribution, and input values reconstruction) (e.g. Belis et al., 2014,

277 Paatero, 2000). All these parameters were evaluated and 5-8 factors were identified as best choices.
278 Nevertheless, mathematics is not enough to determine the right number of factors and the
279 possibility of data interpretation guides the definitive choice (Hopke, 2016; Paatero, 2000). Finally,
280 the 7-factor solution was identified as the best one. The effects of different choices for factor
281 number will be discussed at the end of the paragraph.
282 Factor profiles (total mass of each species normalised to the mass in the factor) and the percent of
283 the species associated to each factor, as well as the mass size distribution of the factors were
284 represented in Figure 4. The mass size distribution was represented both using histogram
285 representation of the ME-2 output and mode representation obtained from data inversion and modes
286 retrieval. In this way, it was possible gaining information on the mass modes GMADs and modes
287 relative contribution to each factor (Table 2). Detailed size-segregated profiles were reported in
288 Figure 5 with histogram representation of the size-segregated relative contribution of the species to
289 the identified factors. In Figure 5, normalisation was carried out to the total average concentration
290 of each species (analogous to percent species for size-segregated representation). Results given in
291 Figure 4, Figure 5, and Table 2 were the bases for factor identification, as explained in the
292 following. Mode-segregated source apportionment for the whole campaign was summarised in
293 Figure 6.
294 The factor identified as "wood burning" was an important contributor to levoglucosan (37%) and at
295 a lesser extent K, well-known tracers for this source, as well as for $SO_4^=$ which was identified as
296 directly emitted by both wood and pellets burning in the literature (e.g. Chandrasekaran et al., 2011;
297 Iinuma et al., 2007). In Figure 5, the contribution of these species was detected also in the ultrafine
298 range and their presence related to residential wood burning as mentioned before. Wood burning
299 factor accounted for 13% of the measured mass. The mass was mainly concentrated in the
300 condensation and droplet modes (96% in total), whereas the remaining 4% was in the Aitken mode.
301 It should be noticed that the mass associated to this source has to be considered as accounting only
302 for local (urban) wood burning contribution. Indeed, a regional contribution from wood burning
303 should be also expected, as 36% of levoglucosan was associated to the regional aerosol factor (see
304 later).
305 The factor identified as "industry" was the main contributor to Zn (35%), which has been identified
306 as a marker for industrial emissions in previous works in the area (e.g. Bernardoni et al., 2011b;
307 Marcazzan et al., 2003). The industry factor accounted on average for 8% of the measured mass.
308 Most of the mass (58%) was contained in the condensation mode, this being among the main
309 contributors to the mass measured in this mode (18%).
310 The factor identified as "resuspended dust" was an important contributor to Ti (27%) and Ca (21%)
311 concentrations. Nevertheless, also components of anthropogenic origin were present and the factor

size distribution was characterised in nearly equal parts by fine (<1μm) and coarse particles (54% and 46%, respectively), thus suggesting that anthropogenic particles previously deposited in the ground are resuspended (e.g. by atmospheric agents) together with soil particles. This factor accounted on average for 13% of the measured mass, and it was one of the two main contributors to the coarse mode and very large particles (22%).

The factor identified as "regional aerosol" was the main single contributor to the measured concentration of nitrate (52%), sulphate (35%), and ammonium (49%). It can be assumed that these ions were entirely in the form of ammonium sulphate and ammonium nitrate as they were chemically balanced in the profile within 5%. As previously mentioned, this factor was responsible for high contributions to levoglucosan (36%) and K (24%) (tracers for wood burning), and to Fe (22%) and Cu (22%) (tracers for traffic) indicating that this factor was not only associated to secondary aerosol, but also to non-local (aged) contributions from primary sources. The regional aerosol factor was the main contributor to the total measured mass (31%) and to the droplet mode (50%), where 81% of the mass of the factor was found. No contribution from the regional aerosol factor was registered in the Aitken mode, mainly because particles in such mode are typically associated to fresh emissions and tend to coagulate towards the accumulation mode in short times. Particle aging further increases particle size, thus justifying the predominance of the droplet mode. Therefore, the absence of a contribution in the Aitken mode and the small contribution to the condensation mode (9%) were further confirmations of the regional origin of this factor.

The factor identified as "construction works" was the main single contributor to the Ca measured concentrations (31%). An association between Ca and construction works at the sampling site was already identified in previous works (Bernardoni et al., 2011b; Vecchi et al., 2009). Its average contribution to the measured mass was 7%. This factor contributed to 22% of the mass measured in the coarse and very large particle modes, where 49% of the mass associated to this factor was found. The coarse/very large particles contribution was ascribed to soil/construction material movement, whereas the contribution to the other modes was related mainly to construction machinery exhaust. It is noteworthy that construction works were locally carried out at the Department of Physics during the measurements period, thus justifying the high (32%) - and quite unexpected - contribution of construction works to the Aitken mode.

Two factors were associated to traffic sources and named "traffic 1" and "traffic 2". They showed very similar profiles, and they were both important contributors to Fe and Cu (overall 44%), Mn (overall 52%), and Ca (overall 32%). Fe and Cu are widely used as markers for traffic sources in source apportionment studies (Pant and Harrison, 2013; Viana et al., 2008). Mn and Ca are reported to have multiple sources, including traffic. As examples, Crilley et al. (2017) found important contribution of Mn from traffic in PM10, Amato et al. (2011) identified traffic as a major

responsible of Mn concentration in the coarse fraction; Ca is often found in traffic source profiles due to traffic-related resuspension or to the contribution of lubricating oils (Viana et al., 2008). It is noteworthy that the two factors did not represent "traffic exhaust" and "traffic non-exhaust" contributions, as the markers for non-exhaust emissions were present in both factors. As for size distributions, the mass of both factors was mainly concentrated in the two accumulation sub-modes (61% for traffic 1 and 69% for traffic 2). In both factors, 23-24% of the mass of the factor was concentrated in the coarse mode, but traffic 2 showed a further 12% mass contribution to very large particles.

The main differences between the two factor profiles were higher contributions from nitrate, ammonium, Mn, and Ti in traffic 2 and from Zn in traffic 1. Little information is present in the literature for what concerns elemental tracers for gasoline and diesel vehicles separately. Lin et al. (2005) evidenced that diesel emissions contributed more than gasoline to the Zn concentrations in ultrafine particles, whereas gasoline was a stronger emitter of ultrafine Mn and Cu. Wang and Hopke (2013) identified that a "Gasoline vehicle" factor by PMF by analysis on PM2.5 samples collected in California was the main responsible of Mn concentration. Link et al. (2017) reported that vehicles equipped with three-way catalyst system (gasoline and liquid petroleum gasoline) have the potential for forming NH_4NO_3 aerosol rapidly and in high yields in presence of OH radicals. In Figure 7, size-segregated distribution of Cu, Mn, and Zn in traffic 1 and traffic 2 factor profiles are shown in histogram representation. Normalisation was carried out setting to 1 the total mass of the single species in each profile. Log-scale was used also for the y-axis to allow better identification of the species contributions to the small-diameter ($d \leq 155$ nm) cut-off stages (which were in any case a low fraction of the total mass of the species). It is noteworthy that Zn relative contribution in these stages was higher for traffic 1 (7.3% vs. 3.1% in traffic 2), whereas Cu (6.9%) and Mn (3.9%) were higher for the traffic 2 factor (1.0% Cu and 1.3% Mn in traffic1 factor profile). Furthermore, traffic 2 showed 29% contribution from nitrate in the factor profiles (Figure 4).

All these pieces of information gave indication of a tentative assignment of traffic 1 to diesel vehicles and traffic 2 to gasoline vehicles contributions. A more detailed insight into these factors showed that traffic 1 factor accounted for 18% of the total measured mass and it was characterised by 83% relative unexplained mass (i.e. the difference between the mass and the sum of the species in the profile), whereas traffic 2 factor accounted for 10% of the total measured mass but the relative unexplained mass was only 51%. For diesel vehicles not equipped with anti-particulate filter, exhaust emissions are known to be at least one order of magnitude higher than gasoline exhaust emissions (e.g. May et al., 2014). It is noteworthy (e.g. Schauer et al., 2006) that the dominant component in exhaust emissions is carbonaceous material which was not detected in this work. Thus, the stronger exhaust contribution expected for diesel vehicles can justify the higher

382 unexplained mass detected in the traffic 1 factor. Considering that diesel vehicles include also
383 heavy duty vehicles and that such vehicles have a higher potential of dust resuspension, assigning
384 traffic 1 factor to diesel vehicles could justify also the presence of the very large particles in this
385 factor and not in traffic 2.
386 Traffic 1 and traffic 2 overall contributions made traffic the most important source of particle mass
387 in all modes but the droplet one, where the contribution from the regional aerosol factor was
388 dominant. The overall contribution of the two traffic factors (28%) might appear higher than in past
389 studies in the area (e.g. Bernardoni et al., 2011b where a contribution of 16% was reported during
390 wintertime for PM_{10} samples). Nevertheless, in Bernardoni et al. (2011b) most of secondary ions
391 were accounted for in "secondary sulphate" and "secondary nitrates" factors: thus, the other factors
392 (including traffic) included mainly primary contributions. Opposite, in this work the analysis on
393 size-segregated samples showed secondary aerosol to be partially explained by specific urban
394 sources. Amato et al. (2016) presented a source apportionment study on PM_{10} data collected in
395 Milan and found an overall 16% contribution for vehicle exhaust and non-exhaust and further 14%
396 vehicle nitrate contribution from NO_x emission inventory. Thus, the overall traffic contribution
397 resulted very similar to the value obtained in the current work. All these results evidenced the
398 ability of source apportionment applied to size-segregated samples to relate at least part of the
399 secondary aerosol to specific sources.
400 Likely the information on chemical composition in different size classes was exploited by the model
401 to relate primary emissions to rapidly-formed secondary compounds. In the regional aerosol factor
402 only 7% of the total nitrate, 13% of sulphate, and 8% of ammonium were found in the four lowest
403 size-classes. In most of other factors, different size distributions were found for secondary
404 compounds. As examples, focusing on the four lowest size classes in the histograms in figure 5,
405 42% and 41% of the total nitrate in each factor was found in this size range for industry and
406 resuspended dust, respectively, whereas 19% and 17% was found for traffic 1 and wood burning,
407 respectively.
408 For what concerns other possible solutions obtained running the ME-2 model, 6-factor solution was
409 excluded because the contributions from "industry" and "construction works" factors mixed in a
410 unique ("other anthropogenic") factor. Increasing to 8 factors, the additional factor could not be
411 identified, as no chemical species tracer for known sources could be detected.
412 Finally, it should be noticed that the main features of the model output (i.e. separation of local vs.
413 regional contributions; ability to identify separate factors associated to gasoline and diesel vehicles)
414 are related to sample features (i.e. size-segregation and detailed chemical characterisation), thus
415 they are not impacted by meteorological conditions. Nevertheless, the latter can affect the relative

416 contribution of the different sources and must be considered when sampling for monitoring
417 purposes – out of the scope of this manuscript – is carried out.
418
419 **4. Conclusions**
420 A study of size-segregated aerosol sampled by SDI multistage impactor was carried out during
421 wintertime in the Milan urban area, which is located in the Po Valley, one of the major pollution
422 hot-spots in Europe.
423 The samples were characterised for mass concentration, and elemental and inorganic ionic
424 composition. Data inversion by the program MICRON and interpolation by log-normal functions
425 allowed detecting and quantifying aerosol modes. Three or four modal mass size distributions were
426 identified in the samples. In all cases, the highest fraction of the mass was found in the
427 accumulation mode.
428 Similarities in size distributions of source tracers suggested the possibility to perform source
429 apportionment. Three-way source apportionment was performed by implementing the Tucker 1
430 model in ME-2. Seven factors were identified, namely wood burning, industry, resuspended dust,
431 construction works, regional aerosol, traffic 1 and traffic 2. It is interesting to note that in previous
432 studies performed in the area on PM_{10} samples, factors related to primary emissions or secondary
433 formation were identified. Opposite, performing the analysis on size-segregated samples led to the
434 identification of local and regional factors. Indeed, running the model on size-segregated samples
435 allowed ascribing part of the secondary compounds to local factors (e.g. traffic 1 and 2, wood
436 burning) probably due to rapid formation of secondary particles in smaller size classes than
437 secondary particles in regional (aged) aerosol. The regional aerosol factor was characterised by a
438 high presence of secondary compounds, but not-negligible contributions primary source tracers (e.g.
439 Cu, Fe, levoglucosan) were also present. The regional aerosol factor prevailed in the droplet mode,
440 whereas the overall contribution from the two traffic sources dominated in the other size fractions.
441 Further insights into the size-segregated profile suggested that the traffic 1 factor could be likely
442 associated to diesel vehicles and the traffic 2 to gasoline vehicles.
443 It is noteworthy that 3-D source apportionment studies on aerosol separated in a number of size
444 classes are nearly absent in the literature. The study presented here showed the possibility to apply
445 3-D source apportionment studies to samples collected with multistage cascade impactors. Such
446 samples can be analysed with traditional techniques (opposite to high-time resolved samples, which
447 usually require to be analysed at accelerator facilities) and do not need dedicated instrumentation
448 other than the sampler. In perspective, these features open the way to more frequent space-
449 distributed size-segregated source apportionment studies, which are of primary importance to

optimise the effectiveness of future abatement strategies and to improve Earth radiation balance models.

Acknowledgements

This study was partially funded by the INFN experiment MANIA (Metodologie Analitiche Nucleari per Indagini Ambientali - Nuclear Analytical Methodologies for Environmental Research). The authors are grateful to prof. Willy Maenhaut for MICRON tutorial and for providing mode interpolation program.

The authors are grateful to F. Cavaliere and D. Viganò of the Mechanical Workshop of the Physics Department for technical support.

461 **References**

462 Amato, F., Viana, M., Richard, A., Furger, M., Prévôt, A. S. H., Nava, S., Lucarelli, F.,
463 Bukowiecki, N., Alastuey, A., Reche, C., Moreno, T., Pandolfi, M., Pey, J., and Querol, X. (2011).
464 Size and time-resolved roadside enrichment of atmospheric particulate pollutants. Atmospheric
465 Chemistry and Physics, 11, 2917-2931
466
467 Amato, F., Alastuey, A., Karanasiou, A., Lucarelli, F., Nava, S., Calzolai, Escrig A., Monfort E.,
468 Sanfelix V., Gianelle V.L., Colombi C., Alves, C., Custódio, D., Nunes, T., Cerqueira, M., Pio, C.,
469 Eleftheriadis, K., Diapouli, E., Reche, C., Minguillón, M. C., Manousakas, M.-I., Maggos, T.,
470 Vratolis, S., Harrison, R. M., and Querol, X. (2016). Non-exhaust contributions to PM levels in 5
471 EU cities. 10th International Conference on Air Quality - Science and Application, Milan, Italy, 14-
472 18 March 2016. https://drive.google.com/drive/folders/0B2iFZ3L-H5pRbGN4Q2NaeGNmQU0
473
474 Belis, C.A., Larsen, B.R., Amato, F., El Haddad, I., Favez, O., Harrison, R.M., Hopke, P.K., Nava,
475 S., Paatero, P., Prévôt, A., Quass, U., Vecchi, R., and Viana, M. (2014). European Guide on Air
476 Pollution Source Identification with Receptor Models. EUR 26080 – Joint Research Centre –
477 Institute for Environment and Sustainability. Luxembourg: Publications Office of the European
478 Union.
479
480 Bernardoni, V., Cuccia, E., Calzolai, G., Chiari, M., Lucarelli, F., Massabò, D., Nava, S., Prati, P.,
481 Valli, G., and Vecchi, R. (2011a). ED-XRF set-up for size-segregated aerosol samples analysis. X-
482 Ray Spectrometry, 40, 79-87
483
484 Bernardoni, V., Vecchi, R., Valli, G. Piazzalunga, A., and Fermo, P. (2011b). PM10 source
485 apportionment in Milan (Italy) using time-resolved data. The Science of the Total Environment,
486 409, 4788-4795
487
488 Bonazza, A., Sabbioni, C., and Ghedini, N. (2005). Quantitative data on carbon fractions in
489 interpretation of black crusts and soiling on European built heritage. Atmospheric Environment, 39,
490 2607-2618
491
492 Bukowiecki, N., Hill, M., Gehrig, R., Lienemann, P., Zwicky, C. N., Hegedüs, F., Falkenberg, G.,
493 Weingartner, E., and Baltensperger, U. (2005). Trace metals in ambient air: hourly size segregated
494 mass concentrations determined by synchrotron-XRF. Environmental Science and Technology, 39,
495 5754–5762

Cabada, J.C., Rees, S., Takahama, S., Khlystov, A., Pandis, S.N., Davidson, C.I., and Robinson, A.L. (2004). Mass size distributions and size resolved chemical composition of fine particulate matter at the Pittsburgh supersite. Atmospheric Environment, 38, 3127-3141

Cahill, T.A. (1996). Climate Forcing by Anthropogenic Aerosols: The Role for PIXE. Nuclear Instruments and Methods in Physics Research B: Beam Interactions with Materials and Atoms, 109/110, 402-406

Chandrasekaran, S.R., Laing, J.R., Holsen, T.M., Raja, S., and Hopke, P.K. (2011). Emission Characterization and Efficiency Measurements of High-Efficiency Wood Boilers. Energy Fuels, 25, 5015–5021

Corsini, E., Vecchi, R., Marabini, L., Fermo, P., Becagli, S., Bernardoni, V., Caruso, D., Corbella, L., Dell'Acqua, M., Galli, C.L., Lonati, G., Ozgen, S., Papale, A., Signorini, S., Tardivo, R., Valli, G., and Marinovich, M. (2017). The chemical composition of ultrafine particles and associated biological effects at an alpine town impacted by wood burning. Science of the Total Environment, 587-588, 223-231

Crilley, L.R., Lucarelli, F., Bloss, W.J., Harrison, R.M., Beddows, D.C., Calzolai, G., Nava, S., Valli, G., Bernardoni, V., and Vecchi, R. (2017). Source apportionment of fine and coarse particles at a roadside and urban background site in London during the 2012 summer ClearfLo campaign. Environmental Pollution, 220, 766-778

EPA (2014). EPA Positive Matrix Factorization (PMF) 5.0 Fundamentals and User Guide. EPA/600/R-14/108, April 2014. https://www.epa.gov/sites/production/files/2015-02/documents/pmf_5.0_user_guide.pdf

Harshman, R. A. and Lundy, M. E. (1994). PARAFAC – Parallel Factor-Analysis. Computational Statistics & Data Analysis, 18, 39–72

Heal, M.R., Kumar, P., and Harrison, R.M. (2012). Particles, air quality, policy and health. Chemical Society Reviews, 41, 6606-6630

530 Hillamo, R. E. (1994) Development of inertial impactor size spectroscopy for atmospheric aerosols.
531 Ph.D. thesis
532
533 Hopke, P.K. (2016). Review of receptor modeling methods for source apportionment. Journal of the
534 Air & Waste Management Association, 66, 237-259
535
536 Iinuma, Y., Brüggemann E., Gnauk T., Müller K., Andreae M. O., Helas G., Parmar R., and
537 Herrmann H. (2007). Source characterization of biomass burning particles: The combustion of
538 selected European conifers, African hardwood, savanna grass, and German and Indonesian peat.
539 Journal of Geophysical Research, 112, D08209
540
541 IPCC (2013). Climate Change 2013: The Physical Science Basis. Contribution of Working Group I
542 to the Fifth Assessment Report of the Intergovernmental Panel on Climate Change [Stocker, T.F.,
543 D. Qin, G.-K. Plattner, M. Tignor, S.K. Allen, J. Boschung, A. Nauels, Y. Xia, V. Bex and P.M.
544 Midgley(eds.)]. Cambridge University Press, Cambridge, United Kingdom and New York, NY,
545 USA, 1535 pp
546
547 Kleeman, M.J., Schauer, J. J., and Cass, G. R. (1999). Size and Composition Distribution of Fine
548 Particulate Matter Emitted from Wood Burning, Meat Charbroiling, and cigarettes. Environmental
549 Science and Technology, 33, 3516-3523
550
551 Li, N., Hopke, P.K., Kumar, P., Cliff, S.S., Zhao, Y., and Navasca, C. (2013). Source
552 apportionment of time- and size-resolved ambient particulate matter. Chemometrics and Intelligent
553 Laboratory Systems, 129, 15–20
554
555 Lin, C.-C., Chen, S.-J., Huang, K.-L., Hwang, W.-I., Chang-Chien, G.-P., and Lin, W.-Y. (2005).
556 Characteristics of metals in nano/ultrafine/fine/coarse particles collected beside a heavily Trafficked
557 road. Environmental Science and Technology, 39, 8113–8122
558
559 Link, M.F., Kim, J., Park, G., Lee, T., Park, T., Bin Babar, Z., Sung, K., Kim, P., Kang, S., Soo
560 Kim, J., Choi, Y., Son, J., Lim, H.-J., and Farmer, D.K. (2017). Elevated production of NH4NO3
561 from the photochemical processing of vehicle exhaust: Implications for air quality in the Seoul
562 Metropolitan Region. Atmospheric Environment, 156, 95-101
563
564 Maenhaut, W., Hillamo, R., Mäkelä, T., Jaffrezo, J.-L., Bergin, M.H., and Davidson, C.I. (1996). A

565 new cascade impactor for aerosol sampling with subsequent PIXE analysis. Nuclear Instruments
566 and Methods in Physics Research Section B: Beam Interactions with Materials and Atoms, 109-
567 110, 482-487
568
569 Maenhaut, W., Jaffrezo, J.-L, Hillamo, R.E, Mäkelä, T, and Kerminen, V.-M. (1999). Size-
570 fractionated aerosol composition during an intensive 1997 summer field campaign in northern
571 Finland. Nuclear Instruments and Methods in Physics Research Section B: Beam Interactions with
572 Materials and Atoms, 150, 345-349
573
574 Maenhaut, W., Cafmeyer, J., Dubtsov, S., and Chi, X. (2002). Detailed mass size distributions of
575 elements and species, and aerosol chemical mass closure during fall 1999 at Gent, Belgium.
576 Nuclear Instruments and Methods in Physics Research Section B: Beam Interactions with Materials
577 and Atoms, 189, 238-242
578
579 Marcazzan, G.M., Ceriani M., Valli G., and Vecchi R. (2003). Source apportionment of PM10 and
580 PM2.5 in Milan (Italy) using receptor modelling. Science of the Total Environment, 317, 137-147
581
582 May, A., Nguyen, N., Presto, A., Gordon, T., Lipsky, E., Karve, M., Gutierrez, A., Robertson, W.,
583 Zhang, M., Brandow, C., Chang, O., Chen, S., Cicero-Fernandez, P., Dinkins, L., Fuentes, M.,
584 Huang, S., Ling, R., Long, J., Maddox, C., Massetti, J., McCauley, E., Miguel, A., Na, K., Ong, R.,
585 Pang, Y., Rieger, P., Sax, T., Truong, T., Vo, T., Chattopadhyay, S., Maldonado, H., Maricq, M.,
586 and Robinson, A. (2014). Gas- and particle-phase primary emissions from in-use, on-road gasoline
587 and diesel vehicles. Atmospheric Environment, 88, 247-260
588
589 Ozgen, S., Becagli, S., Bernardoni, V., Caserini, S., Caruso, D., Corbella, L., Dell'Acqua, M.,
590 Fermo, P., Gonzalez, R., Lonati, G., Signorini, S., Tardivo, R., Tosi, E., Valli, G., Vecchi, R., and
591 Marinovich, R. (2017). Analysis of the chemical composition of ultrafine particles from two
592 domestic solid biomass fired room heaters under simulated real-world use. Atmospheric
593 Environment 150, 87-97
594
595 Paatero, P. (1999). The multilinear engine — a table-driven least squares program for solving
596 multilinear problems, including the n-way parallel factor analysis model. Journal of Computational
597 and Graphical Statistics, 8:4, 854-888
598
599 Paatero, P. (2000). User's Guide for the Multilinear Engine Program "ME-2" for Fitting Multilinear

and Quasi-Multilinear Models. University of Helsinki: Helsinki, Finland

Paatero, P. (2015). User's Guide for Positive Matrix Factorization Programs PMF2 and PMF3, Part 1–2: Tutorial. University of Helsinki: Helsinki, Finland (update 31 March 2015)

Pakkanen, T.A., Kerminen, V.-M. K., Korhonen, C.H., Hillamo, R.H., Aarnio, P., Koskentalo, T., and Maenhaut, W. (2001). Use of atmospheric elemental size distributions in estimating aerosol sources in the Helsinki area. Atmospheric Environment, 39, 5363-5374

Pant, P., and Harrison, R.M. (2013). Estimation of the contribution of road traffic emissions to particulate matter concentrations from field measurements: A review. Atmospheric Environment, 77, 78-97

Peré-Trepat, E., Kim, E., Paatero, P., and Hopke, P.K. (2007). Source apportionment of time and size resolved ambient particulate matter measured with a rotating DRUM impactor. Atmospheric Environment, 41, 5921–5933

Piazzalunga, A., Fermo, P., Bernardoni, V., Vecchi, R., Valli, G., and De Gregorio, M.A. (2010). A simplified method for levoglucosan quantification in wintertime atmospheric particulate matter by high performance anion-exchange chromatography coupled with pulsed amperometric detection. International Journal of Environmental Analytical Chemistry, 90, 934–947.

Piazzalunga, A., Bernardoni, V., Fermo, P., and Vecchi, R. (2013). Optimisation of analytical procedures for the quantification of ionic and carbonaceous fractions in the atmospheric aerosol and applications to ambient samples. Analytical and Bioanalytical Chemistry, 405, 1123- 1132

Pirjola, L., Niemi, J.V., Saarikoski, S., Aurela, M., Enroth, J., Carbone, S., Saarnio, K., Kuuluvainen, H., Kousa, A., Rönkkö, T., and Hillamo, R. (2017). Physical and chemical characterization of urban winter-time aerosols by mobile measurements in Helsinki, Finland. Atmospheric Environment, 158, 60-75

Polissar, A.V., Hopke, P.K., Paatero, P., Malm, W.C., and Sisler, J.F. (1998). Atmospheric aerosol over Alaska: 2. Elemental composition and sources. Journal of Geophysical Research, 103, 19045-19057

635 Pope, C.A. III, and Dockery, D.W. (2006). Health Effects of Fine Particulate Air Pollution: Lines
636 that Connect. Journal of Air & Waste Management Association, 56, 709-742
637
638 Pöschl, U. (2005). Atmospheric Aerosols: Composition, Transformation, Climate and Health
639 Effects. Angewandte Chemie International Edition, 44, 7520-7540
640
641 Raabe, O.G., Braaten, D.A., Axelbaum, R.L., Teague, S., and Cahill, T. (1988). Calibration studies
642 of the DRUM impactor. Journal of Aerosol Science, 19, 183-195
643
644 Robert, M. A., Kleeman, M.J., and Jakober, C.A. (2007). Size and Composition Distributions of
645 Particulate Matter Emissions: Part 2—Heavy-Duty Diesel Vehicles. Journal of the Air & Waste
646 Management Association, 57, 1429-1438
647
648 Rogula-Kozłowska, W. (2016). Size-segregated urban particulate matter: mass closure, chemical
649 composition, and primary and secondary matter content. Air Quality, Atmosphere and Health, 9,
650 533-550
651
652 Salma, I., Ocskay, R., Raes, N., and Maenhaut, W. (2005). Fine structure of mass size distributions
653 in an urban environment. Atmospheric Environment, 39, 5363-5374
654
655 Schauer, J.J., Lough G.C., Shafer M.M., Christensen W.F., Arndt M.F., DeMinter J.T., and Park, J.-
656 S. (2006). Characterization of Metals Emitted from Motor Vehicles. Research Report 133. Health
657 Effects Institute, Boston MA
658
659 Seinfeld, J.H., and Pandis, S.N. (1998). Atmospheric Chemistry and Physics from air pollution to
660 climate change. New York. John Wiley and Sons, Incorporated
661
662 Simoneit, B.R.T., Schauer, J.J., Nolte, C.G., Oros, D.R., Elias, V.O., Fraser, M.P., Rogge, W.F.,
663 and Cass, G.R. (1999). Levoglucosan, a tracer for cellulose in biomass burning and atmospheric
664 particles. Atmospheric Environment, 33, 173-182.
665
666 Tucker, L. R. (1966). Some Mathematical Notes on 3-Mode Factor Analysis. Psychometrika, 31,
667 279–311
668
669 Ulbrich, I. M., Canagaratna, M. R., Cubison, M. J., Zhang, Q., Ng, N. L., Aiken, A. C., and

Jimenez, J. L. (2012). Three-dimensional factorization of size-resolved organic aerosol mass spectra from Mexico City. Atmospheric Measurement Techniques, 5, 195-224.

Vecchi R., Marcazzan G., Valli G., Ceriani M., and Antoniazzi C. (2004). The role of atmospheric dispersion in the seasonal variation of PM1 and PM2.5 concentration and composition in the urban area of Milan (Italy). Atmospheric Environment, 38, 4437-4446

Vecchi R., Bernardoni V., Fermo P., Lucarelli F., Mazzei F., Nava S., Prati P., Piazzalunga A., and Valli G. (2009). 4-hours resolution data to study PM10 in a "hot spot" area in Europe. Environmental Monitoring and Assessment, 154, 283-300.

Viana, M., Kuhlbusch, T.A.J., Querol, X., Alastuey, A., Harrison, R.M., Hopke, P.K., Winiwarter, W., Vallius, M., Szidat, S., Prévôt, A.S.H., Hueglin, C., Bloemen, H., Wåhlin, P., Vecchi, R., Miranda, A.I., Kasper-Giebl, A., Maenhaut W., and Hitzenberger R. (2008). Source apportionment of particulate matter in Europe: A review of methods and results. Journal of Aerosol Science 39, 827-849

Viidanoja, J., Kerminen, V.-M., and Hillamo, R. (2002). Measuring the size distribution of atmospheric organic and black carbon using impactor sampling coupled with thermal carbon analysis: Method development and uncertainties. Aerosol Science and Technology, 36, 607-616.

Wang Y., and Hopke P.K. (2013). A ten–year source apportionment study of ambient fine particulate matter in San Jose, California. Atmospheric Pollution Research, 4, 398-404

Watson J.G. (2002). Visibility: Science and Regulation. Journal of Air & Waste Management Association 52, 628–713

Wolfenbarger, J.K., and Seinfeld, J.H. (1990). Inversion of size distribution data. Journal of Aerosol Science, 21, 227-247

Figure captions

Figure 1: example of modes reconstruction: a) histogram representation obtained from data measured on each impaction stage; b) data inversion by the program MICRON; c) modes interpolation. The example is referred to the mass size distribution of one of the collected samples.

Figure 2: average type 1 and type 2 mass size distributions

Figure 3: average size distribution for secondary ions (a), wood burning markers (b), traffic markers (c)

Figure 4: left panel: factor profiles (black bars) and percent species (grey dots); right panel: factor mass size distributions

Figure 5: histogram representation of the size-segregated relative contribution of the species to the identified factors. Normalisation was carried out to the total average concentration of each species. For each species, x-axis represents log(d_p) and the x-axis scale is the same as histograms in figure 1 and figure 4. Cut-off size for each represented stage (i.e. left-end of coloured bars) are reported in the legend.

Figure 6: mode-segregated source apportionment. Sum of percentages is 100%±1% due to number rounding.

Figure 7: histogram representation of size-segregated distribution of (a) Cu, (b) Mn, and (c) Zn in the traffic 1 and traffic 2 factors profile. Normalisation to the total concentration of the species to each factor profile was carried out. For each component, x-axis represents log(d_p) and the x-axis scale is the same as histograms in figure 1 and figure 4. Cut-off size for each represented stage (i.e. left-end of coloured bars) are reported in the legend.

Table 1: geometric mean aerodynamic diameter (GMAD), relative mass concentration (RMC), and relative number of cases of mode presence (n.cases) for Aitken, condensation, droplet, coarse modes and very large particles. RMC evaluation was limited to the cases in which the mode was present.

	Aitken mode			**Condensation mode**			**Droplet mode**			**Coarse mode**			**Very large particles**		
	GMAD (µm)	**RMC (%)**	**n. cases (%)**	**GMAD (µm)**	**RMC (%)**	**n. cases (%)**	**GMAD (µm)**	**RMC (%)**	**n. cases (%)**	**GMAD (µm)**	**RMC (%)**	**n. cases (%)**	**GMAD (µm)**	**RMC (%)**	**n. cases (%)**
S				0.28	30%	86%	0.66	59%	100%	3.4	17%	71%			
Cl				0.36	18%	86%	0.72	29%	71%	4.4	61%	100%	16.1	10%	36%
K				0.26	31%	86%	0.58	46%	100%	3.7	25%	100%	15.7	9%	29%
Ca										3.9	79%	100%	15.7	11%	86%
Ti				0.22	5%	36%				3.5	71%	100%	15.1	13%	64%
Cr				0.31	17%	36%	0.67	38%	57%	2.9	64%	100%	4.7	29%	29%
Mn				0.30	13%	43%	0.72	42%	100%	3.2	50%	100%	15.7	10%	21%
Fe				0.42	6%	21%				3.2	74%	100%	16.6	7%	43%
Ni				0.28	21%	43%	0.48	45%	86%	3.0	50%	93%			
Cu				0.27	6%	71%				3.0	72%	100%	16.3	7%	21%
Zn				0.27	14%	79%	0.77	49%	93%	2.7	43%	100%	14.5	9%	14%
Levoglucosan	0.10	4%	100%	0.32	56%	100%	0.63	43%	78%	1.6	5%	78%	5.2	3%	78%
K^+	0.10	4%	44%	0.29	49%	89%	0.62	37%	89%	1.9	4%	22%	4.1	12%	89%
NO_3^-	0.11	2%	100%	0.31	28%	100%	0.71	61%	100%	2.4	6%	67%	4.0	10%	56%
$SO_4^=$	0.10	4%	100%	0.29	31%	100%	0.67	52%	100%	1.69	8%	56%	4.5	10%	100%
NH_4^+	0.10	2%	89%	0.31	35%	100%	0.70	62%	100%	3.5	2%	44%	8.2	1%	67%

732 *Table 2: geometric mean aerodynamic diameter (GMAD) and mode relative mass contribution (RMC) to each factor.*

Factor name		Aitken mode	Condensation submode	Droplet submode	Coarse mode	Very large particles
Wood Burning	**GMAD (µm)**	0.036	0.210	0.599		
	Relative contribution	4%	24%	72%		
Industry	**GMAD (µm)**	0.105	0.298		1.31	6.39
	Relative contribution	6%	58%		17%	19%
Resuspended Dust	**GMAD (µm)**		0.292	0.586	2.99	9.15
	Relative contribution		33%	23%	34%	10%
Regional	**GMAD (µm)**		0.203	0.695	2.81	
	Relative contribution		9%	81%	10%	
Construction works	**GMAD (µm)**	0.034	0.189	0.567	2.61	7.53
	Relative contribution	11%	14%	25%	12%	37%
Traffic 1	**GMAD (µm)**	0.118	0.344	0.98	2.97	9.30
	Relative contribution	5%	28%	33%	23%	12%
Traffic 2	**GMAD (µm)**	0.094	0.286	0.823	4.18	
	Relative contribution	7%	31%	38%	24%	

733

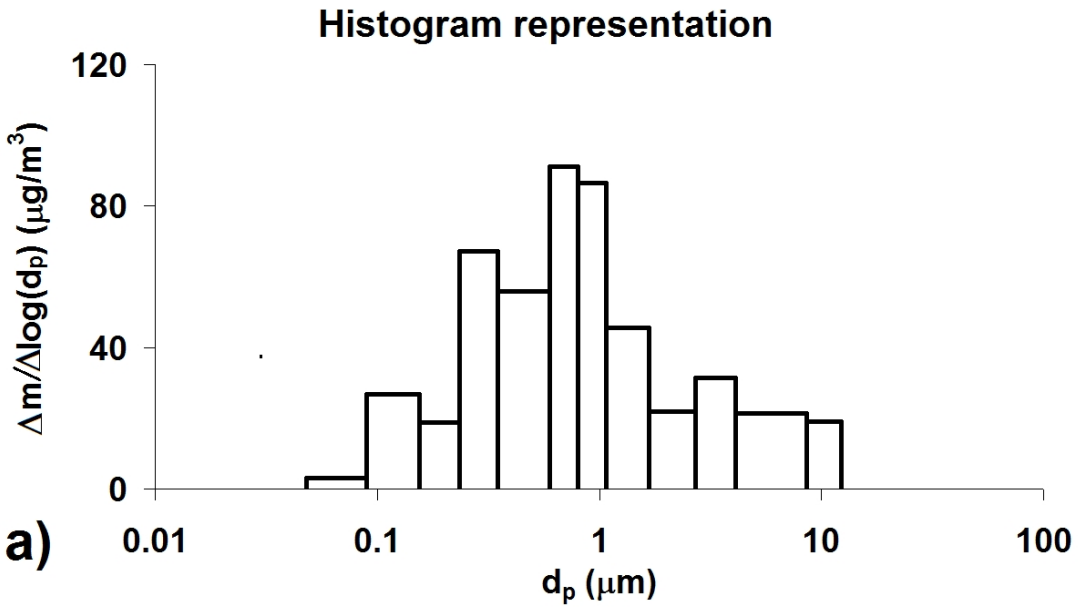
Histogram representation
120
80
40
0
Δm/Δlog(dp) (μg/m3)
0.01
0.1
1
10
100
dp (μm)

a)

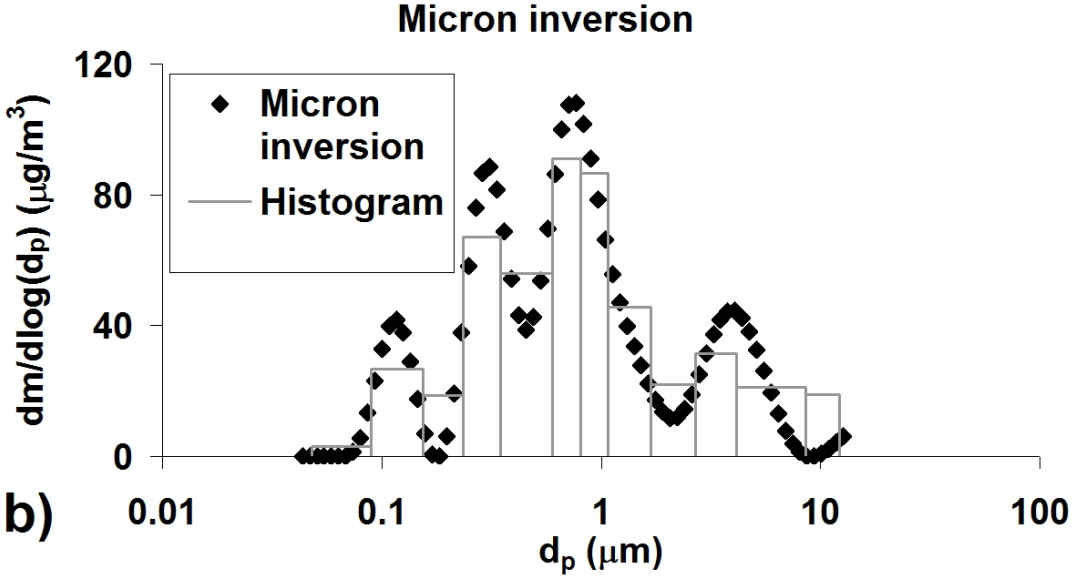
Micron inversion
Micron inversion
Histogram
120
80
40
0
dm/dlog(dp) (μg/m3)
0.01
0.1
1
10
100
dp (μm)

b)

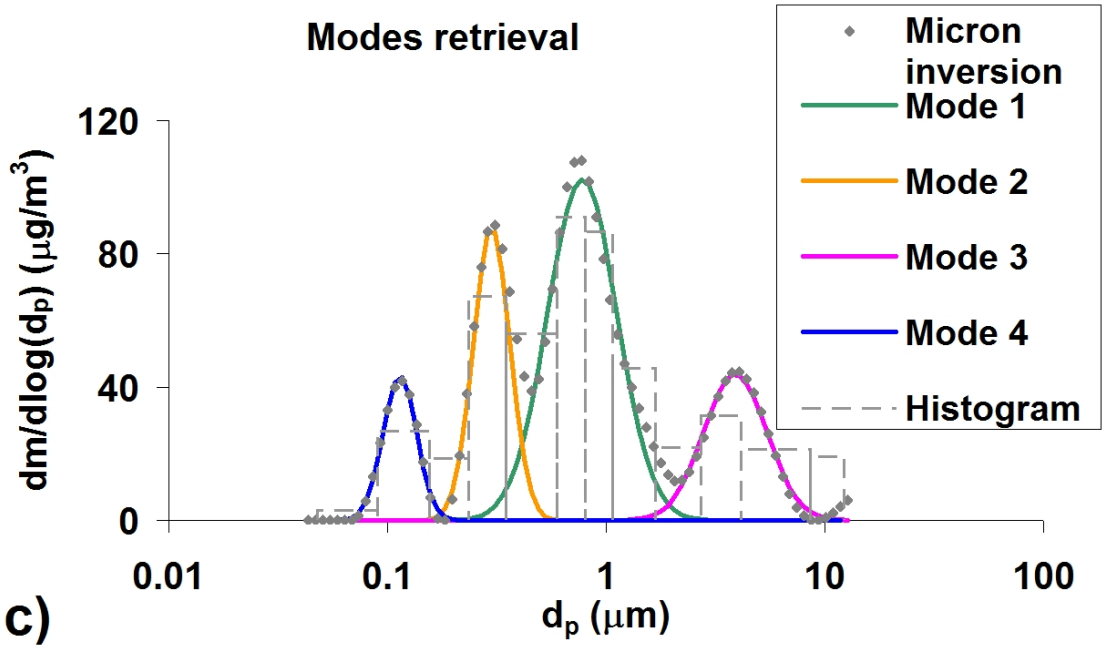
Modes retrieval
Micron inversion
Mode 1
Mode 2
Mode 3
Mode 4
Histogram
120
80
40
0
dm/dlog(dp) (μg/m3)
0.01
0.1
1
10
100
dp (μm)

c)

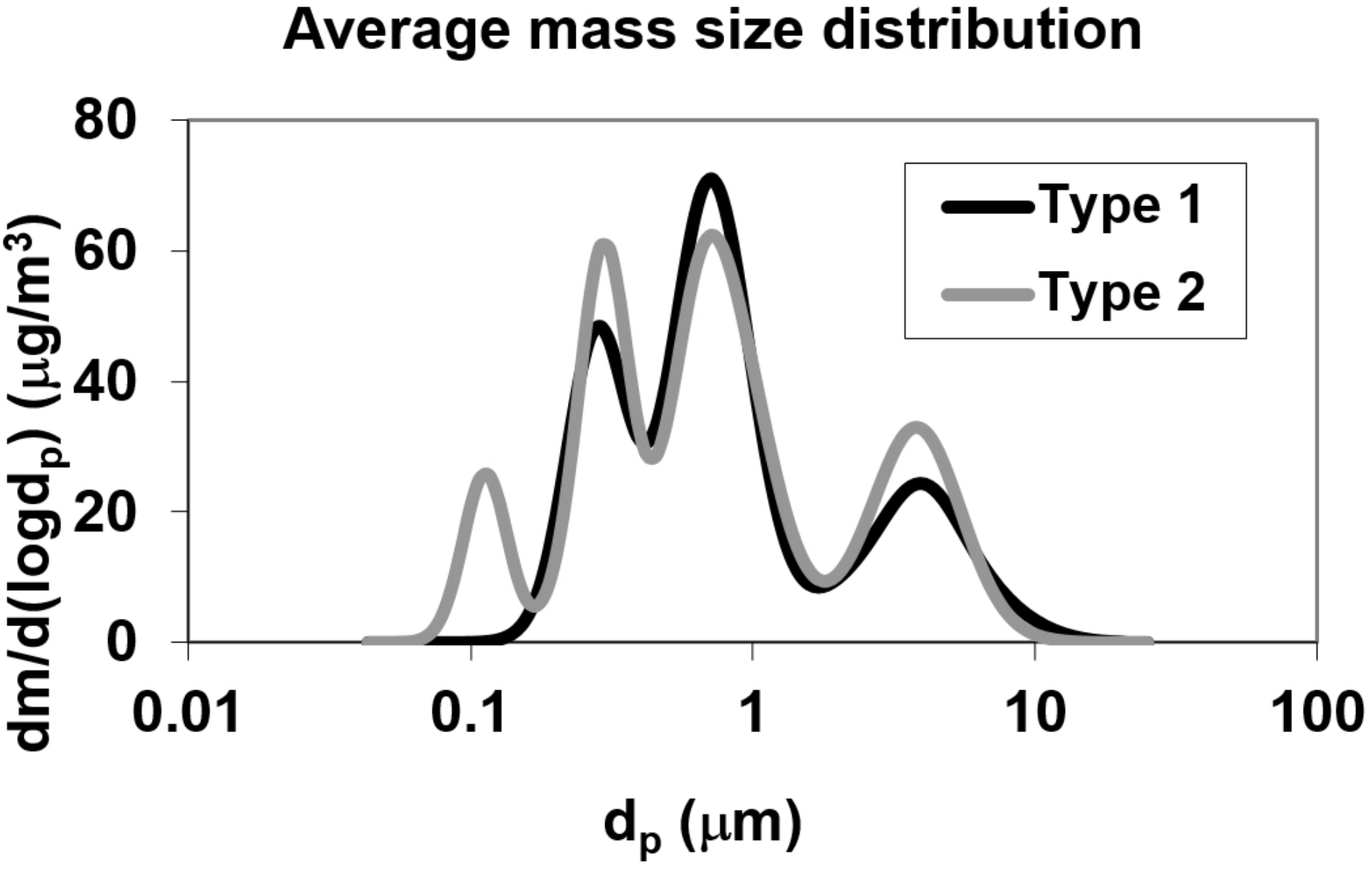
Average mass size distribution
80
60
40
20
0
dm/d(logd$_p$) (μg/m^3)
0.01
0.1
1
10
100
d$_p$ (μm)
Type 1
Type 2

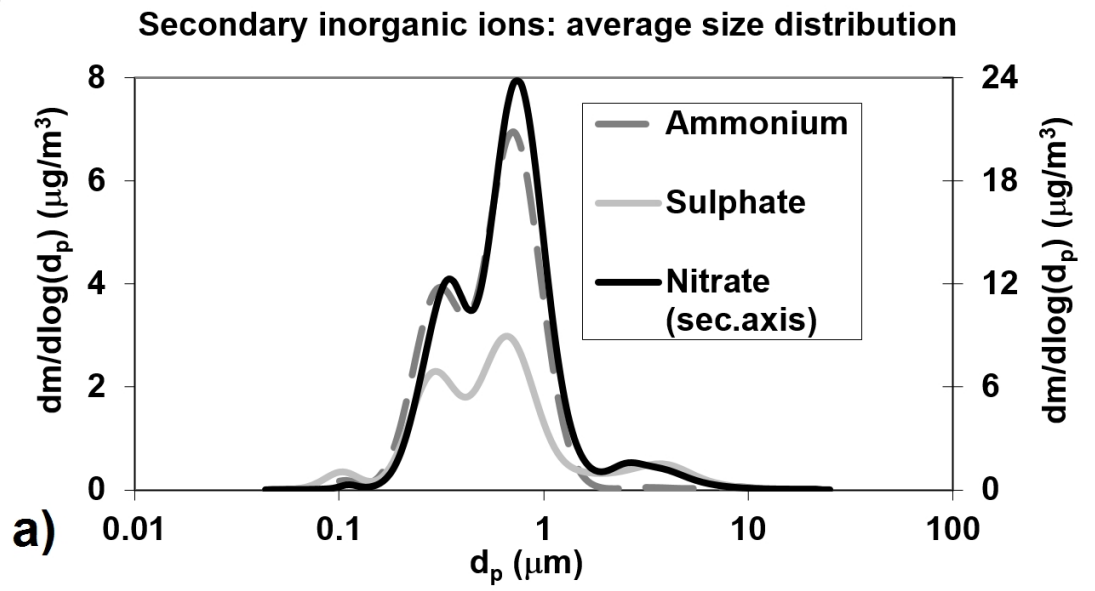
Secondary inorganic ions: average size distribution
Ammonium
Sulphate
Nitrate (sec.axis)
dm/dlog(dp) (μg/m3)
dm/dlog(dp) (μg/m3)
dp (μm)
a)

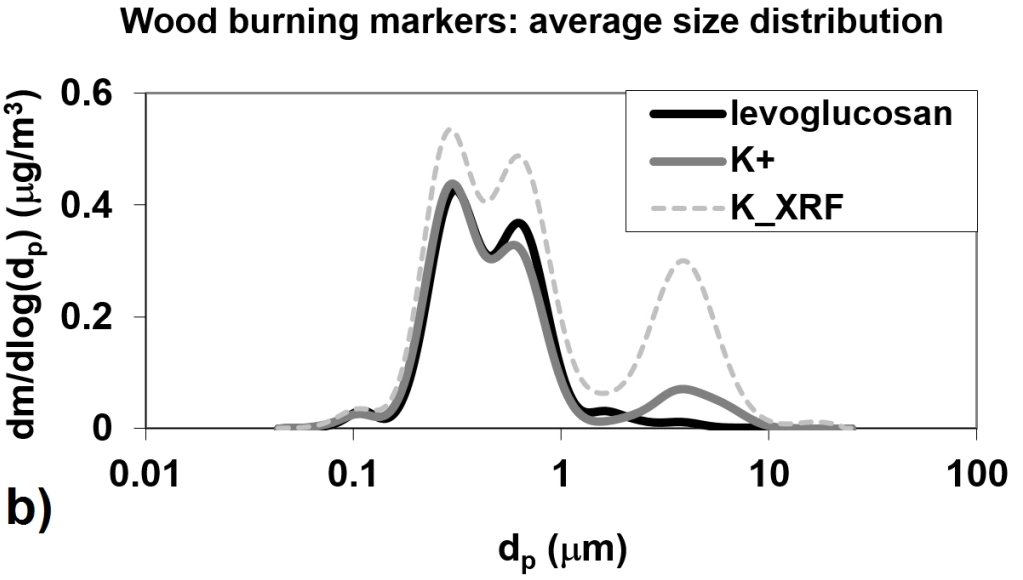
Wood burning markers: average size distribution
levoglucosan
K+
K_XRF
dm/dlog(dp) (μg/m3)
dp (μm)
b)

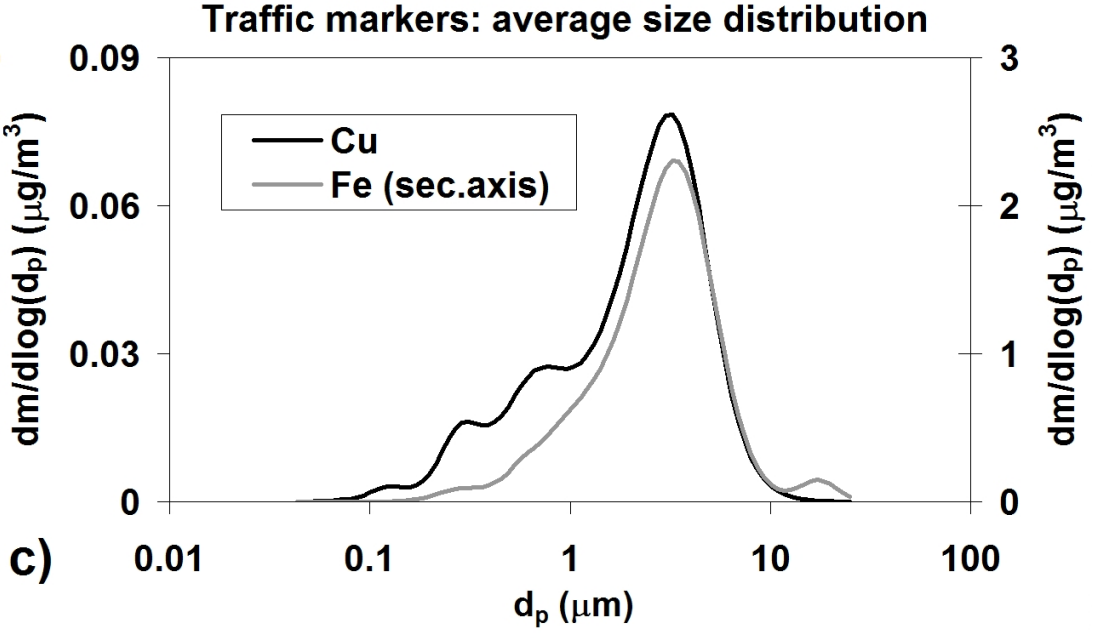
Traffic markers: average size distribution
Cu
Fe (sec.axis)
dm/dlog(dp) (μg/m3)
dm/dlog(dp) (μg/m3)
dp (μm)
c)

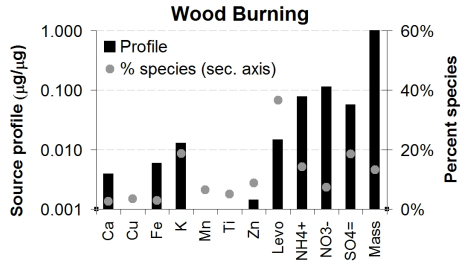
Wood Burning
Profile
% species (sec. axis)
Source profile (µg/µg)
Percent species
1.000
0.100
0.010
0.001
60%
40%
20%
0%
Ca
Cu
Fe
K
Mn
Ti
Zn
Levo
NH4+
NO3-
SO4=
Mass

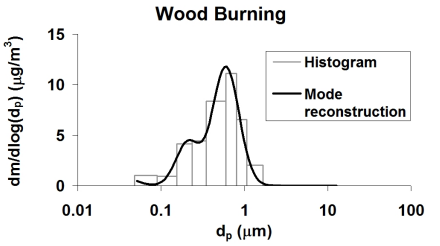
Wood Burning
Histogram
Mode reconstruction
dm/dlog(dp) (µg/m3)
dp (µm)
15
10
5
0
0.01
0.1
1
10
100

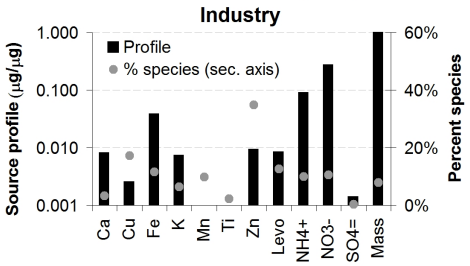
Industry
Profile
% species (sec. axis)
Source profile (µg/µg)
Percent species
1.000
0.100
0.010
0.001
60%
40%
20%
0%
Ca
Cu
Fe
K
Mn
Ti
Zn
Levo
NH4+
NO3-
SO4=
Mass

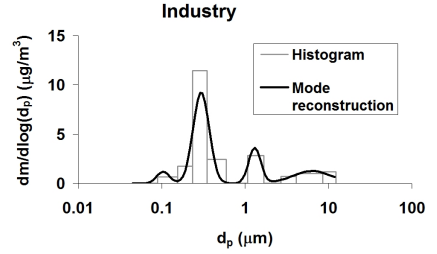
Industry
Histogram
Mode reconstruction
dm/dlog(dp) (µg/m3)
dp (µm)
15
10
5
0
0.01
0.1
1
10
100

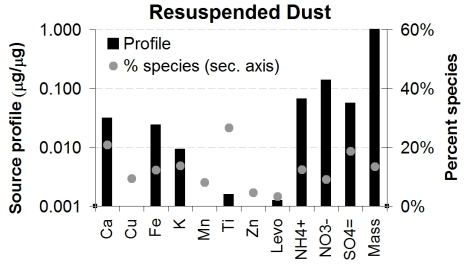
Resuspended Dust
Profile
% species (sec. axis)
Source profile (µg/µg)
Percent species
1.000
0.100
0.010
0.001
60%
40%
20%
0%
Ca
Cu
Fe
K
Mn
Ti
Zn
Levo
NH4+
NO3-
SO4=
Mass

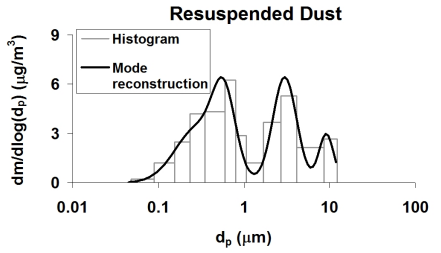
Resuspended Dust
Histogram
Mode reconstruction
dm/dlog(dp) (µg/m3)
dp (µm)
9
6
3
0
0.01
0.1
1
10
100

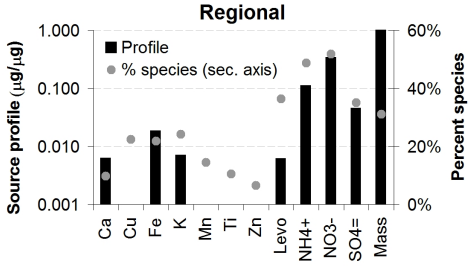
Regional
Profile
% species (sec. axis)
Source profile (µg/µg)
Percent species
1.000
0.100
0.010
0.001
60%
40%
20%
0%
Ca
Cu
Fe
K
Mn
Ti
Zn
Levo
NH4+
NO3-
SO4=
Mass

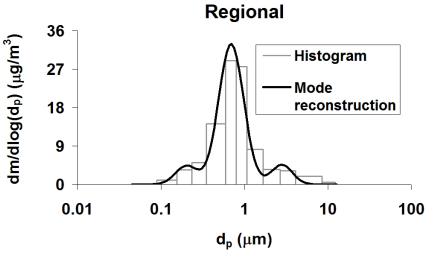
Regional
Histogram
Mode reconstruction
dm/dlog(dp) (µg/m3)
dp (µm)
36
27
18
9
0
0.01
0.1
1
10
100

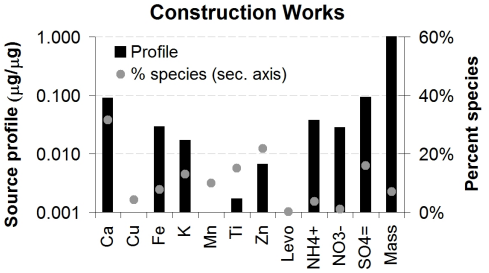
Construction Works
Profile
% species (sec. axis)
Source profile (µg/µg)
Percent species
1.000
0.100
0.010
0.001
60%
40%
20%
0%
Ca
Cu
Fe
K
Mn
Ti
Zn
Levo
NH4+
NO3-
SO4=
Mass

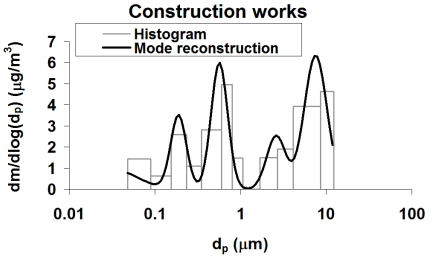
Construction works
Histogram
Mode reconstruction
dm/dlog(dp) (µg/m3)
dp (µm)
7
6
5
4
3
2
1
0
0.01
0.1
1
10
100

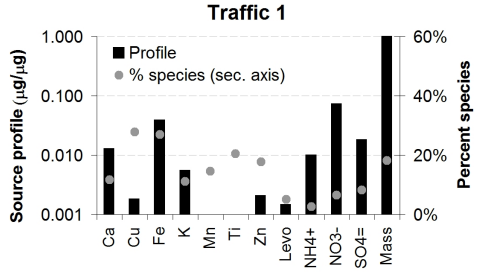
Traffic 1
Profile
% species (sec. axis)
Source profile (µg/µg)
Percent species
1.000
0.100
0.010
0.001
60%
40%
20%
0%
Ca
Cu
Fe
K
Mn
Ti
Zn
Levo
NH4+
NO3-
SO4=
Mass

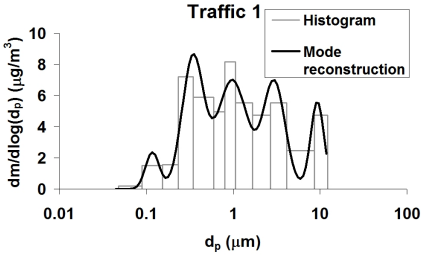
Traffic 1
Histogram
Mode reconstruction
dm/dlog(dp) (µg/m3)
dp (µm)
10
8
6
4
2
0
0.01
0.1
1
10
100

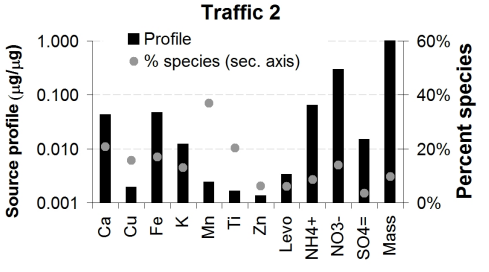
Traffic 2
Profile
% species (sec. axis)
Source profile (µg/µg)
Percent species
1.000
0.100
0.010
0.001
60%
40%
20%
0%
Ca
Cu
Fe
K
Mn
Ti
Zn
Levo
NH4+
NO3-
SO4=
Mass

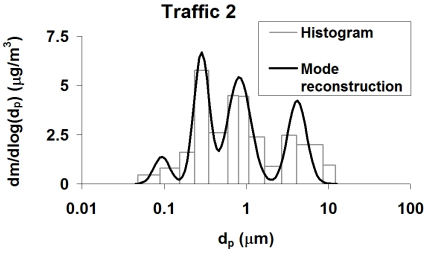
Traffic 2
Histogram
Mode reconstruction
dm/dlog(dp) (µg/m3)
dp (µm)
7.5
5
2.5
0
0.01
0.1
1
10
100

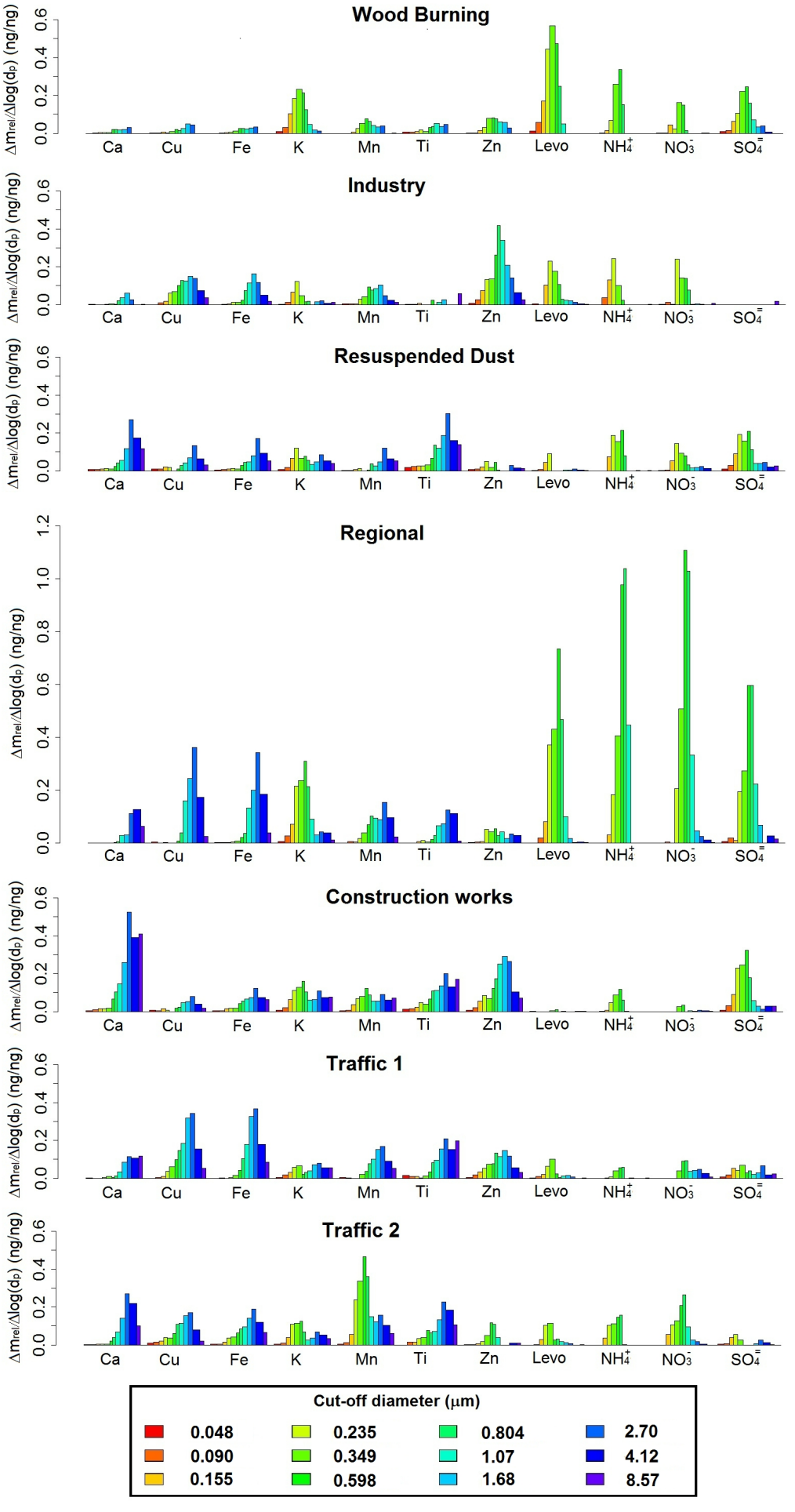
Wood Burning
Industry
Resuspended Dust
Regional
Construction works
Traffic 1
Traffic 2
Δmrel/Δlog(dp) (ng/ng)
Ca
Cu
Fe
K
Mn
Ti
Zn
Levo
NH4+
NO3-
SO4=
Cut-off diameter (μm)
0.048
0.090
0.155
0.235
0.349
0.598
0.804
1.07
1.68
2.70
4.12
8.57

AITKEN MODE

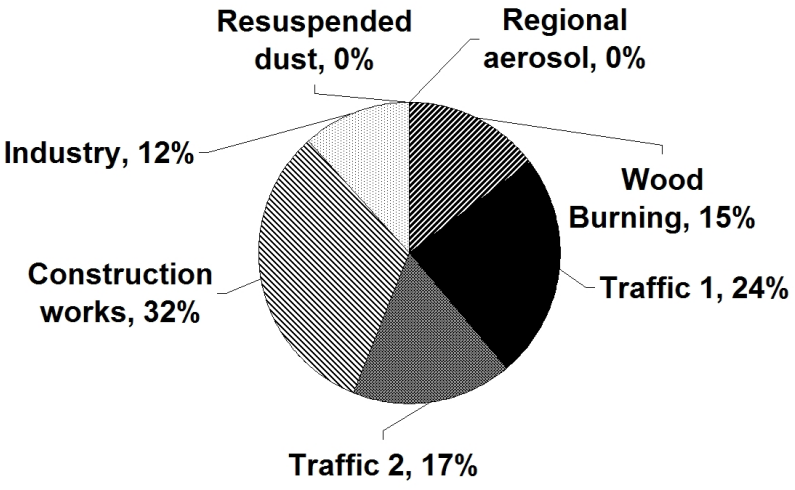

CONDENSATION MODE

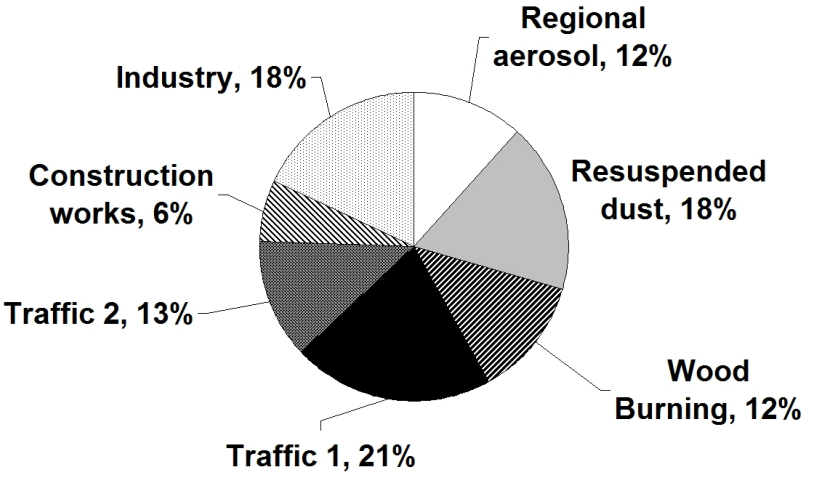

DROPLET MODE

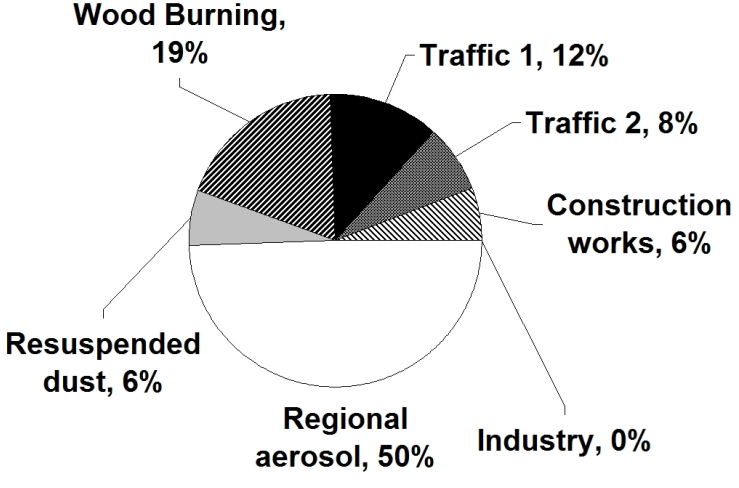

COARSE MODE AND VERY LARGE PARTICLES

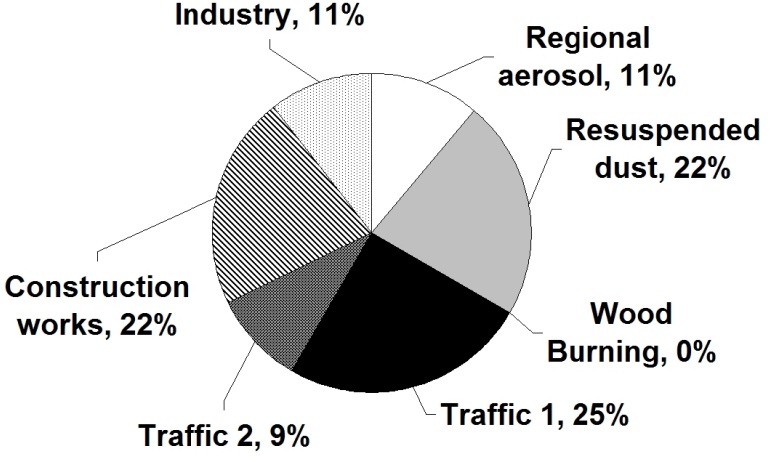

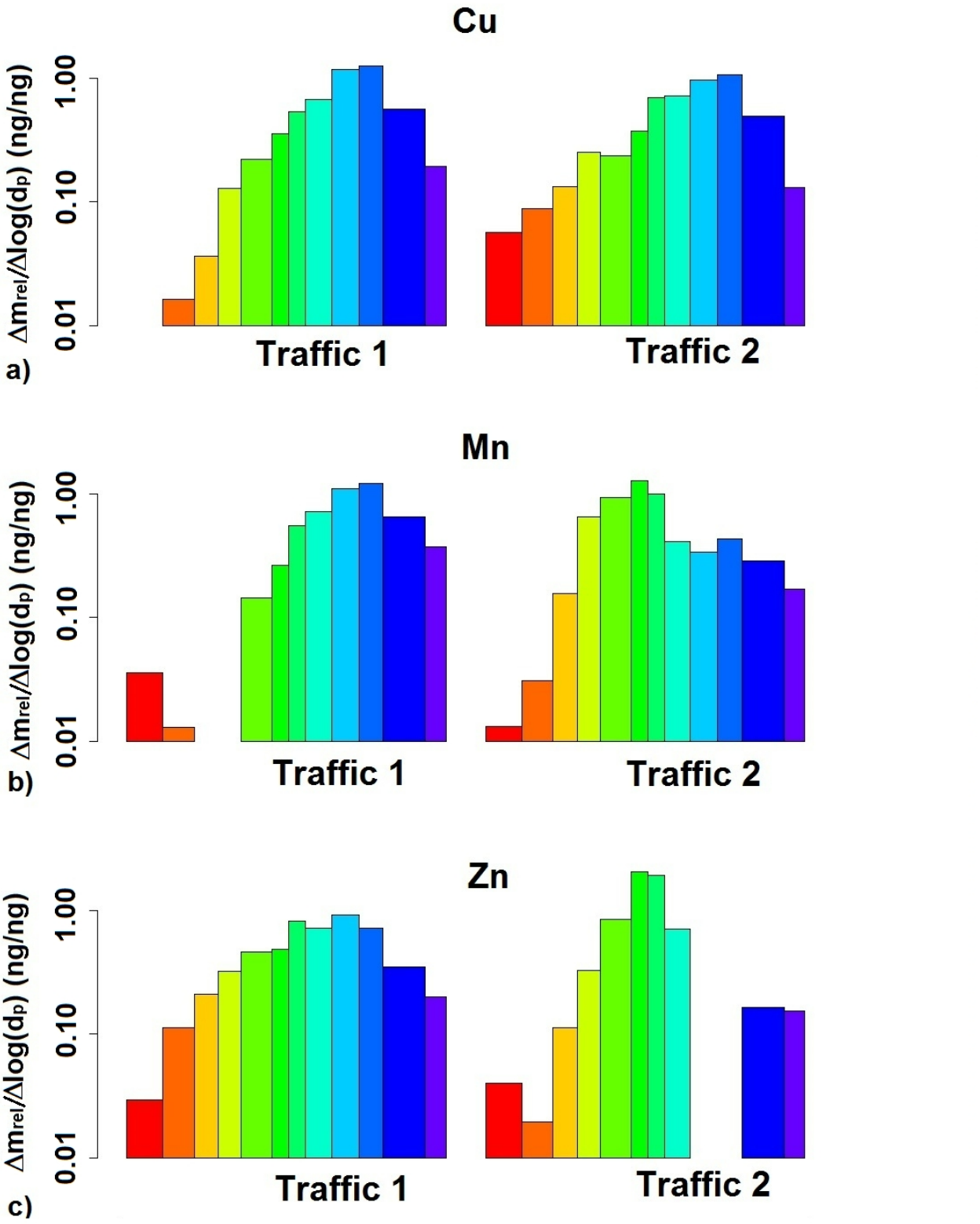
Cu
Mn
Zn
$\Delta m_{rel}/\Delta \log(d_p)$ (ng/ng)
0.01
0.10
1.00
a)
b)
c)
Traffic 1
Traffic 2
Cut-off diameter (μm)
0.048
0.090
0.155
0.235
0.349
0.598
0.804
1.07
1.68
2.70
4.12
8.57